

Article

Measurement Method of Refractive Index for Optical Lenses Based on Curvature Radius Fitting of Small-Sized Aspheric Surfaces

Tao Zhong ^{1,2}, Guangyan Guo ^{2,*}, Yasong Chow ^{1,2}, Yixuan Yang ¹, Tianhao Zhang ³, Jiru Yang ¹, Mingxuan Lu ², Yonghuan Wang ¹, Yongjian Zhu ², Tianlei Jia ³, Yishi Shi ² and Changjun Ke ²

- ¹ College of Physics and Electronic Engineering, Chongqing Normal University, Chongqing 401331, China; zt2640135642@163.com (T.Z.); cchow9908@gmail.com (Y.C.); earnestyx@outlook.com (Y.Y.); yangjiru08@163.com (J.Y.); wyh_16vkj@163.com (Y.W.)
- ² Aerospace Information Research Institute, Chinese Academy of Sciences, No. 9 Deng Zhuang South Road, Beijing 100094, China; lumx@aircas.ac.cn (M.L.); 13659893243@163.com (Y.Z.); optsys@gmail.com (Y.S.); kecj@aircas.ac.cn (C.K.)
- ³ School of Mathematics and Physics Science and Engineering, Hebei University of Engineering, Handan 056038, China; heu_zhangtianhao@163.com (T.Z.); 13303098505@163.com (T.J.)
- * Correspondence: guogy@aircas.ac.cn

Abstract: The study of the refractive index of traditional lenses is one of the foundational topics in the field of optics. The refractive index of a lens determines its ability to refract and focus light, making it a key parameter in optical design and applications. For the measurement of the refractive index of blind samples of finished lenses, this paper proposes a measurement method based on the use of a focal length measuring instrument and an aspheric profilometer to measure the surface shape data of the front and back surfaces of the lens. This method combines curve fitting algorithms and curvature radius fitting algorithms, ultimately reconstructing the lens model using Zemax and back-calculating the refractive index of the lens. For the samples employed in this paper, the measurement accuracy of the focal length can achieve 1.06%, the fitting accuracy of the curvature radius can reach 0.138%, and the recovery accuracy of the refractive index can attain $6.303 \times 10^{-4}\%$.



Academic Editor: Valerio Pinchetti

Received: 3 December 2024

Revised: 7 January 2025

Accepted: 13 January 2025

Published: 20 January 2025

Citation: Zhong, T.; Guo, G.; Chow, Y.; Yang, Y.; Zhang, T.; Yang, J.; Lu, M.; Wang, Y.; Zhu, Y.; Jia, T.; et al. Measurement Method of Refractive Index for Optical Lenses Based on Curvature Radius Fitting of Small-Sized Aspheric Surfaces. *Optics* **2025**, *6*, 4. <https://doi.org/10.3390/opt6010004>

Copyright: © 2025 by the authors. Licensee MDPI, Basel, Switzerland. This article is an open access article distributed under the terms and conditions of the Creative Commons Attribution (CC BY) license (<https://creativecommons.org/licenses/by/4.0/>).

Keywords: aspheric; curvature radius fitting; leveling algorithm; reverse modeling; refractive index

1. Introduction

The use of aspheric elements in optical systems can correct aberrations, improve imaging quality, and reduce system size. Traditional research on the refractive index [1] of lenses primarily focuses on material selection, the optimization of fabrication processes, and the relationship between refractive index and optical performance. The advent of advanced materials science has led to the incorporation of a plethora of novel substances in lens fabrication, most of which exhibit superior refractive indices and optical characteristics, thereby expanding the potential for future lens production. Recent endeavors have been directed towards developing methodologies for ascertaining the refractive index of lenses without compromising their surface integrity. Utilizing the immersion technique, several refractive index measurement strategies have been introduced. For instance, reference [2] details a procedure in which the lens under examination is submerged in a fluid with an adjustable refractive index until parity with the lens's refractive index is achieved. This approach, which deduces the lens's refractive index from that of the fluid, is fraught

with constraints that hinder its broad application. It necessitates the identification of an appropriate fluid medium that resists absorption, a task that is both laborious and fraught with experimental variability. Achieving consistent results often entails numerous iterative trials to discern the fluid's imaging behavior. Alternative methods for refractive index determination have been proposed, circumventing the need for miscible immersion. These include the utilization of the Murty shearing interferometer [3], Ronchi gratings [4], acousto-optic gratings [5], the Fabry–Perot etalon [6], the Moiré deflection measurement [7], and Fourier transform spectroscopy [8], all of which expedite the measurement process. While these techniques obviate the need for repetitive experimentation, the fidelity of the liquid index measurement remains a critical determinant of the method's efficacy, with the accuracy of the refractive index measurement being contingent upon the precision of the liquid index assessment.

In 2003, Li Chao [9] and others introduced the phenomena of spherical reflection imaging and refraction–reflection–refraction imaging observed in the determination of the focal length of crescent-shaped thin lenses, pointing out that these phenomena can be used to accurately determine the refractive index and the curvature radii of the front and back surfaces. In 2004, Zheng Shiwang [10] proposed a simple method based on the geometric optics spherical formula, which can derive the curvature radii and refractive index of thin lenses. In 2011, Xu Jianli [11] observed the spherical reflection imaging of biconcave thick lenses, and using this experimental phenomenon in conjunction with the object–image formula, measured the curvature radii and refractive index of the front and back surfaces of biconcave thick lenses. In 2013, Lingfeng et al. [12] proposed a non-immersive lens refractive index measurement method based on fiber point diffraction longitudinal interference. If the object point is located at the vertex of the front surface, the lens imaging process simplifies to a single refraction at the back surface. The refractive index of the lens is obtained by measuring its thickness, the curvature radius of the back surface, and the distances between the object point and the image point. Experiments have shown that this method achieves an accuracy better than 2.2×10^{-4} , and aspheric lenses can also be accurately measured using this method. In 2019, HD Ford et al. [13] combined confocal scanning with low-coherence interferometry to provide remote measurements of the refractive index and thickness of transparent materials. Additionally, the refractive index can be derived by measuring multiple parameters of the lens using Michelson interferometry [14], digital holographic interferometry [15], and laser differential confocal techniques [16].

The above methods have significant limitations, including high operational difficulty, complexity, and time consumption. This article proposes a method for obtaining the refractive index of a lens by inversely reconstructing the aspheric model based on the focal length and curvature radius. To ensure the generality of the experimental process and the accuracy and repeatability of the results, we used lenses with different curvature aspheric profiles, including short focal length, long focal length, biconvex, and plano-convex shapes. The test results indicate that this method is universal and highly precise. The measurement accuracy of this experiment is high, and it has good operability and low cost. This method not only allows for the measurement of the refractive index of blind samples, but also has practical guiding significance for the design, optimization, and manufacturing processes of various lenses, whether involving single aspheric lenses or aspheric lens groups.

2. Experimental Methods and Principles

2.1. Measurement Method for Lens Focal Length

The focal length of a lens is an important parameter for determining the object–image relationship, and the accuracy of its measurement directly affects the debugging and use

of the entire optical system. Compared to conventional-sized lenses, the focal length measurement of small-sized aspheric samples requires higher clamping precision and measurement accuracy. As the aspheric surface has multiple points of curvature variation outside of the central curvature position, multiple focal points often exist when testing the entire effective aperture of the sample. Therefore, an aperture stop is added to limit the effective aperture, allowing for precise measurement of the focal length.

2.2. Measurement Method for Curvature Radius of Aspheric Surfaces

2.2.1. Measurement of Aspheric Surface Profile Curves

Aspheric optical elements are those whose surface shape deviates from that of a sphere. Due to the limitations of the measurement adjustment mechanism of the aspheric profilometer, it cannot ensure that when the probe passes through the center of the sample, multiple scans can be conducted near the vertex of the sample during the peak-finding process (e.g., rotating the sample stage by 90°). The measurement yields multiple surface profile curves of the same sample with different effective apertures; among these curves, the one with the largest aperture is selected as the actual curve representing the aspheric profile of the lens. The test results are shown in Figure 1.

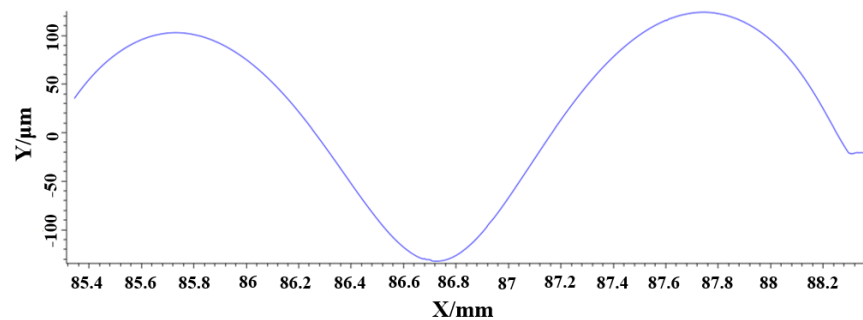


Figure 1. Non-spherical profilometer measuring lens surface curve.

2.2.2. Fitting of Aspheric Curvature Radius

The aspheric surface is primarily measured based on its shape and parameters. The surface shape refers to the three-dimensional distribution of the surface in the spatial domain. The measurement result of the surface shape is a geometric quantity. The optical axis passing through the vertex of the aspheric lens surface curve is designated as the y-axis, while the direction perpendicular to the optical axis is designated as the x-axis. The surface curve comprises multiple discrete points (x, y). The fitting formula can be generally divided into the basic shape section (including paraxial curvature c and conic constant k), the high-order correction section (including high-order coefficients a_4, a_6, \dots, a_{20}), and the longitudinal correction section (offset b). This form of fitting formula can flexibly describe various complex aspheric shapes and its fitting effect can be optimized by adjusting the parameters. The aspheric formula is as follows:

$$y = \frac{cx^2}{1 + \sqrt{1 - (k+1)c^2x^2}} + \sum_{i=2}^n a_{2i}x^{2i} + b \quad (1)$$

Standard data from patent examples have been selected to generate standard curves using the above aspheric fitting formulas. The generated standard curves are perfectly flat, so no leveling preprocessing is required. As shown in Figure 1, for surface profiles with smaller curvature radii, the fitted curvature radius values are obtained by varying the fitting interval range. By comparing these values with the true values from the patent examples, the maximum fitting error is found to be $\Delta R_{\max} = -0.000256819$ mm, as shown in Figure 2a,d. For surface profiles with larger curvature radii, the maximum fitting error

is $\Delta R_{\max} = -0.02009724$ mm, as shown in Figure 2b,e. For surface profiles with multiple points of curvature change, the maximum fitting error is $\Delta R_{\max} = -0.000332606$ mm, as shown in Figure 2c,f. Repeated fitting was conducted for the surface profiles with varying curvatures, and the fitting errors remained consistent.

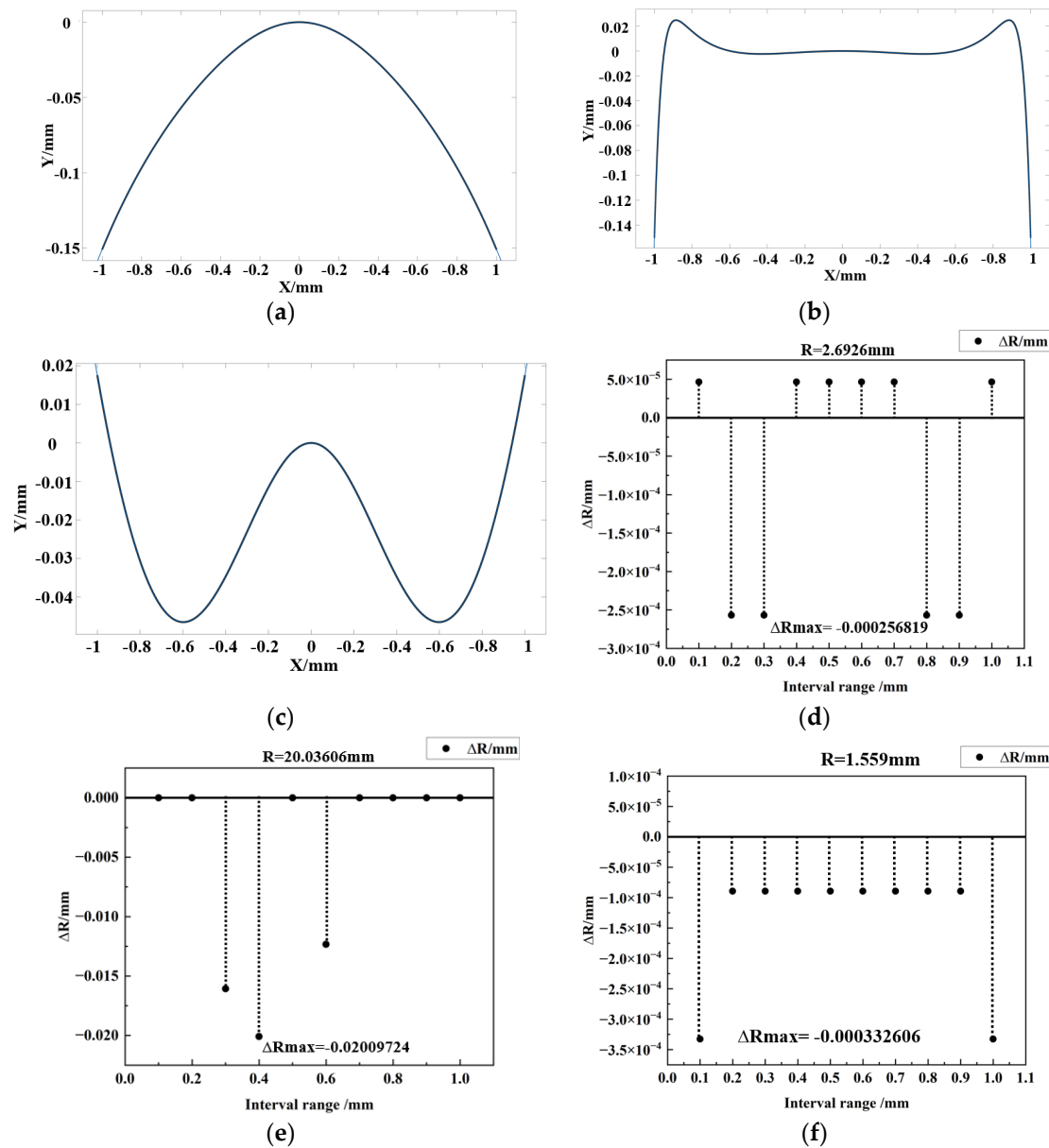


Figure 2. Fitting results of three different surface profiles in various interval ranges: (a,d) show the fitting results for surface profiles with smaller curvature radii across different intervals; (b,e) show the fitting results for surface profiles with larger curvature radii across different intervals; (c,f) show the fitting results for surface profiles with multiple points of curvature change across different intervals.

However, the actual profile curves measured by the aspheric profilometer exhibit a certain degree of tilt, and due to the measurement accuracy of the instrument, it cannot be guaranteed that the curves are perfectly flat. Therefore, before fitting the aspheric curvature radius, it is necessary to level the curves first.

(a) Curve Leveling and Symmetry Preprocessing

The curves measured by an aspheric profilometer are often tilted, and the apex of the aspheric surface does not lie at the origin of the coordinate system. However, for even-order

aspheric curves that are axisymmetric, it is necessary to select a symmetric fitting interval in order to accurately fit the curvature at the same cross-section. If the curve is not leveled, the fitting curvature errors can be significant, or fitting errors may occur. Therefore, leveling the surface profile curves measured by the aspheric profilometer is crucial for surface fitting. To address this issue, this paper proposes an algorithm for an evaluation function that uses the rotation angle of the symmetry axis and the horizontal and vertical translations of the curve as variables, setting a leveling precision to adjust the apex of the initially scanned tilted curve to the origin of the coordinate system, ensuring that the curve is symmetric about the Y-axis.

(b) Fitting Accuracy Evaluation Metrics

R^2 , adjusted R^2 , RMSE, and SSE are used as evaluation metrics for the accuracy of surface fitting. R^2 is a statistical measure of the goodness-of-fit, also known as the coefficient of determination, with values ranging from 0 to 1. The closer the value of R^2 is to 1, the better the regression line fits the observed values.

$$R^2 = 1 - \frac{SSE}{SST} \quad (2)$$

In this context, SSE is the sum of squared errors, and SST is the total sum of squares.

Adjusted R^2 is a modification of R^2 . When additional variables are added to a model, R^2 typically increases, even if the added variables do not contribute meaningfully to the model. Adjusted R^2 corrects for this by introducing a term that accounts for the number of variables in the model. The closer the value of adjusted R^2 is to 1, the better the fit of the model. The expression is as follows:

$$Adjust R^2 = 1 - \left(1 - R^2\right) \frac{n - 1}{n - p - 1} \quad (3)$$

The root mean square error (RMSE) is the square root of the mean square error (MSE). A smaller RMSE indicates a better fit of the model to the data. The expression is as follows:

$$RMSE = \sqrt{\frac{SSE}{n}} \quad (4)$$

The sum of squared errors (SSE) calculates the difference in the sum of the squares of the errors between the fitted data and the corresponding points of the original data. The closer the SSE is to 0, the better the model selection and fit, and the more successful the data prediction. The expression is as follows:

$$SSE = \sum_{i=1}^n \left(y_i - \tilde{y}\right)^2 \quad (5)$$

(c) Fitting Method for Radius of Curvature

After the curve is flattened, repeated fitting is performed by changing the fitting interval multiple times. The fitting results can yield coefficients for the cone, radius of curvature, and higher-order even aspheric terms, among others. The cone coefficient is a parameter that describes the similarity between the aspheric shape and a cone; it not only determines the shape characteristics of the asphere but also affects the optical performance and application effectiveness of the asphere. Higher-order even aspheric terms are beneficial for aberration correction, improving image quality, and enhancing the performance of optical systems. Among these factors, the radius of curvature has the most significant impact on the numerical model restoration of the refractive index. It describes the degree to which the lens or mirror surface deviates from a straight line, that

is, its degree of curvature. For aspheric lenses, the radius of curvature changes with the distance from the optical axis, which is a key feature distinguishing it from spherical lenses. Different materials have different refractive indices, and variations in the refractive index can affect the design of the curvature radius of the lens. Therefore, when designing and manufacturing lenses, it is essential to consider the relationship between the radius of curvature, focal length, and refractive index to ensure that the optical performance of the lens meets its application requirements.

Due to the impact of flattening accuracy, the aspheric surface cannot be adjusted to an absolute flat state, resulting in certain errors. Thus, a standard surface shape is rotated by a certain angle, and under the condition of being unable to achieve absolute flatness, the radius of curvature R is adjusted by changing the fitting range in different intervals to verify the reliability of the fitting. As shown in Figure 3.

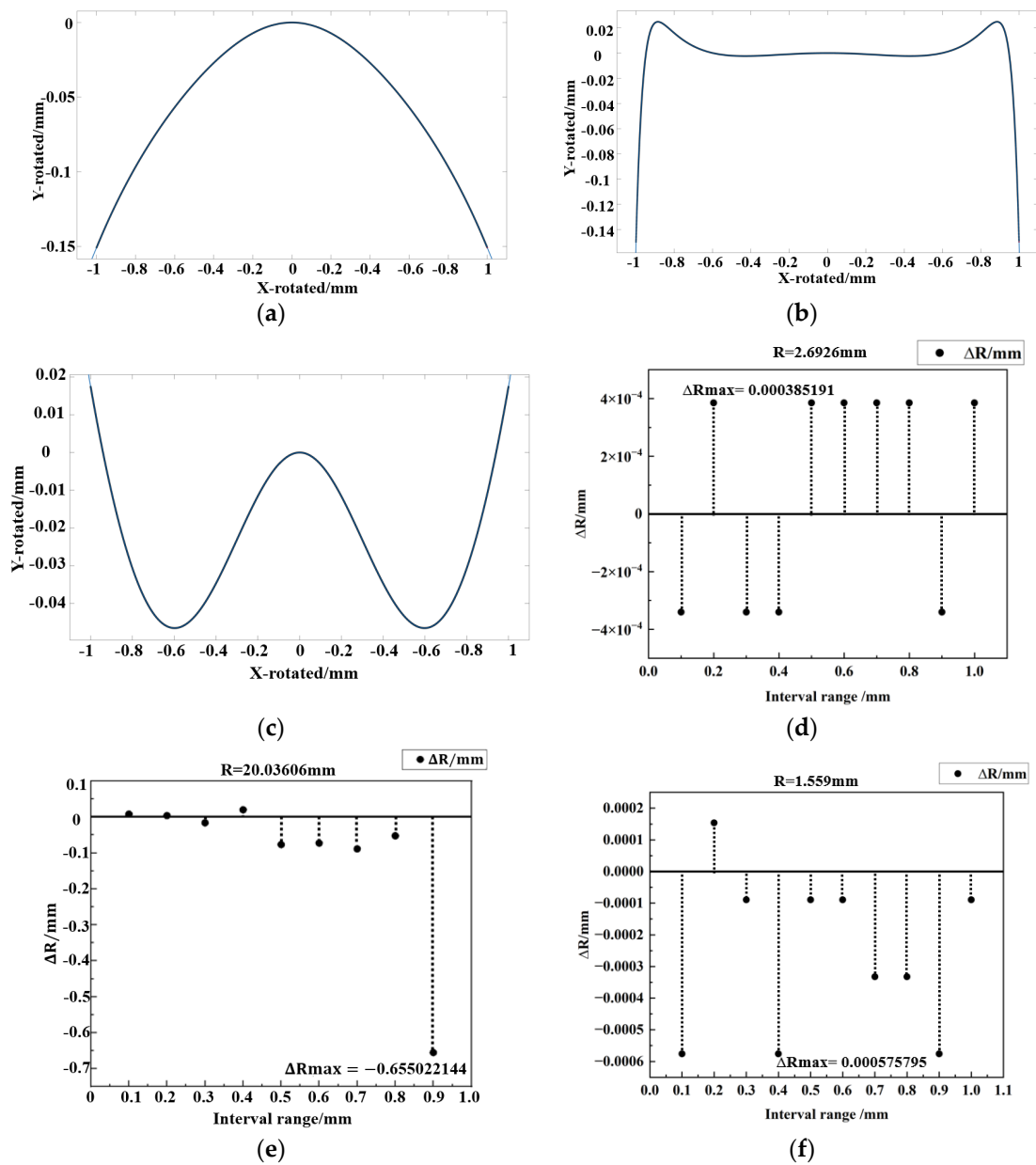


Figure 3. Cont.

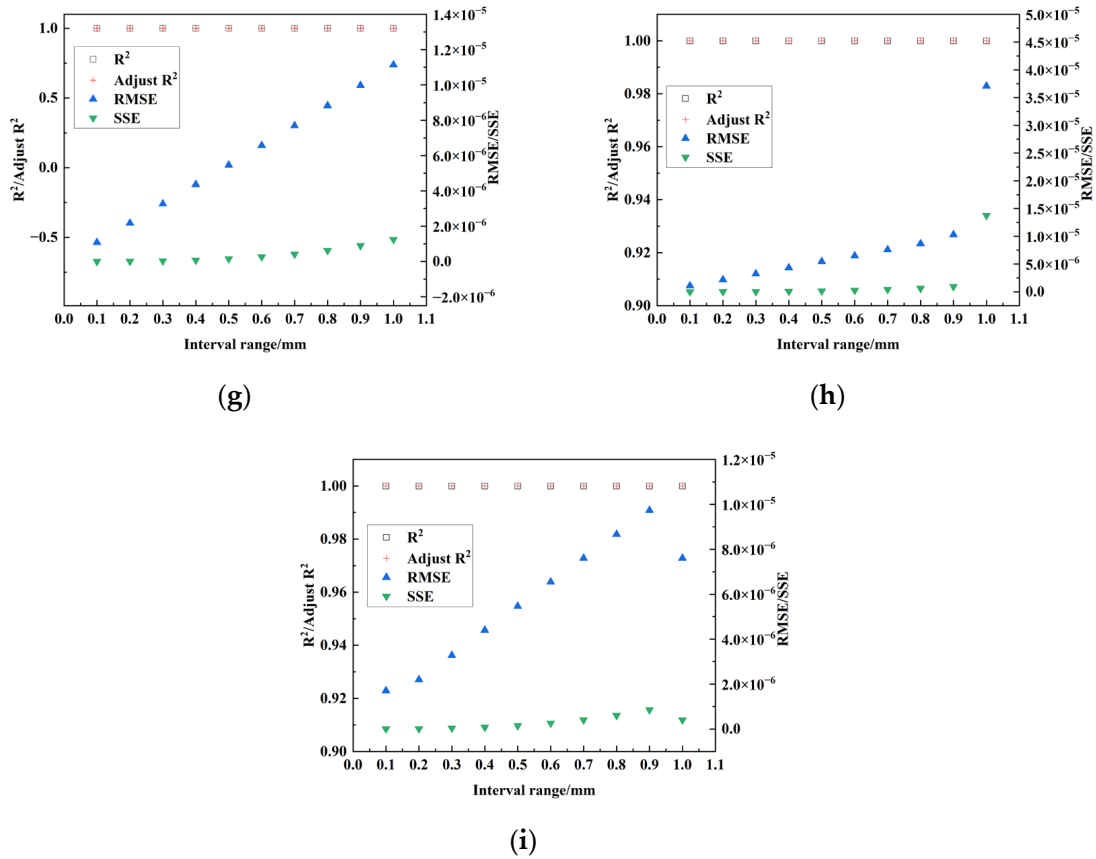


Figure 3. Fitting results of three standard surface shapes after rotating by a certain angle across different interval ranges; (a,d,g) show the fitting results and goodness-of-fit evaluation indicators for surface shapes with smaller radii of curvature across different intervals; (b,e,h) present the fitting results and goodness-of-fit evaluation indicators for surface shapes with larger radii of curvature across different intervals; (c,f,i) depict the fitting results and goodness-of-fit evaluation indicators for surface shapes with multiple variable curvature points across different intervals.

From the analysis of the above fitting data, it can be concluded that under the rotation at flattening accuracy, the fitting errors of the radii of curvature are all greater than the fitting errors of the standard curve when absolutely flat. For surface shapes with larger radii of curvature, the fitting error is $\Delta R_{\max} = -0.655022144$ mm; for surface shapes with smaller radii of curvature, the fitting error is $\Delta R_{\max} = 0.000385191$ mm; and for surface shapes with multiple variable curvature points, the fitting error is $\Delta R_{\max} = 0.000575795$ mm. The fitting data for the rotated surface shapes indicate that, given the current flattening accuracy, the induced fitting error of the radius of curvature is within an acceptable range, and has little impact on subsequent numerical model restoration.

After rotation, both the SSE and RMSE of the different surface shapes are less than 10^{-5} , indicating a high degree of fitting, with a smaller difference between the predicted values and the actual values. Additionally, the R^2 and adjusted R^2 values across the different fitting intervals are all equal to 1, demonstrating that the model has a strong explanatory power regarding the observed data, resulting in better fitting outcomes.

2.3. Inverse Numerical Model Restoration of Refractive Index

In the process of determining the refractive index of a blind sample lens, the accuracy of the measurement can be confirmed by calculating the refractive index using the focal length, radius of curvature, and refractive index formulas from geometric optics. Generally,

thick lenses are commonly used, and the focal length f of a thick lens with a thickness of d can be expressed as follows:

$$\frac{1}{f} = (n - 1) \left(\frac{1}{R_1} - \frac{1}{R_2} \right) + \left(\frac{d}{n} \right) \frac{(n - 1)^2}{R_1 R_2} \quad (6)$$

After obtaining the two key data points of focal length and radius of curvature, the refractive index of the aspheric lens can be derived through an inverse numerical model. By comparing the refractive index calculated using the thick lens formula with the refractive index obtained from the inverse model restoration, the correctness of the experiment can be verified.

3. Experiment and Data Analysis

In the experiment, the standard samples used were the aspheric AC90754 plano-convex lens, the AC91558 plano-convex lens, and the AC111116 double-convex lens, and their focal lengths and aspheric surface shape data were tested.

3.1. Focal Length Measurement Results

A parallel light beam was passed through the sample lens and a collimating lens, then imaged onto the optical tube's image plane. The focal point was accurately positioned using a displacement stage, allowing for the calculation of the effective focal length of the sample. The accurate determination of the image point on the image plane after the light beam passes through the sample and collimating lens directly affects the accuracy of the measurement results. However, due to precision issues during the molding and processing stages, there exists an error compared to the design value of the focal length. By carrying out the measurement multiple times and calculating the average, the focal length data obtained for AC90754, AC91558, and AC111116 were $f_1 = 4.856$ mm, $f_2 = 18.204$ mm, and $f_3 = 2.716$ mm, respectively.

3.2. Surface Profile Measurement

The surface profile data were measured using a Taylor Hobson PGI 1240 profilometer. This instrument is suitable for the optical measurement of aspheric surfaces ranging from small to medium sizes, with measurements being virtually unaffected by the steepness of the aspheric surface, and the maximum edge measurement angle reaching 85° . The measured surface profile data shown in Figure 4 below:

3.3. Radius of Curvature Fitting

3.3.1. Leveling and Selection of Curves

To define the function, the original test curve requires a horizontal translation distance dx , a vertical translation distance dy , and a rotation angle $\Delta\theta$. For the discrete points on the curve, the leveling process ensures symmetry about the y -axis. Upper and lower limit thresholds are defined to find the closest positive and negative x values on the curve. As shown in Figure 5. Next, a leveling evaluation function Q is defined as follows:

$$Q = \sum_{i=0}^n |y(x_i) - y(-x_i)| \quad (7)$$

where n is the radius of the lens. For each point, the x -values that are opposite with respect to the y -axis are used to minimize the horizontal coordinate difference between the two points. The cumulative sum is then computed to minimize the value of Q . A minimized Q value indicates that the curve has been leveled, as shown in Figure 6.

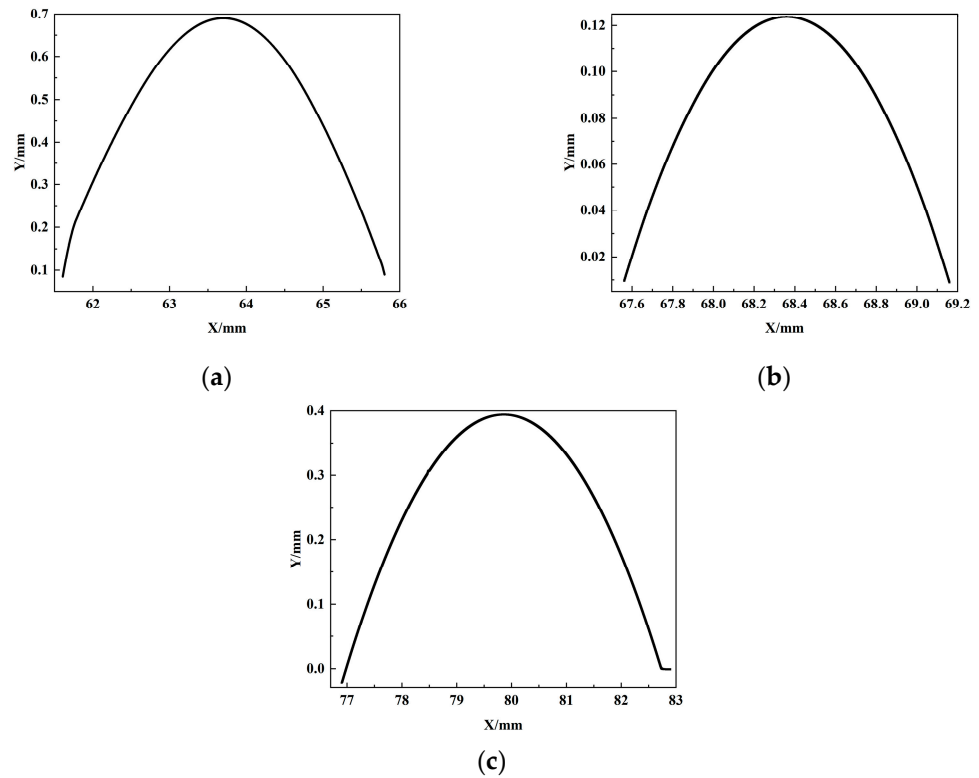


Figure 4. (a–c) are the surface profile curve graphs for AC111116, AC90754, and AC91558, respectively.

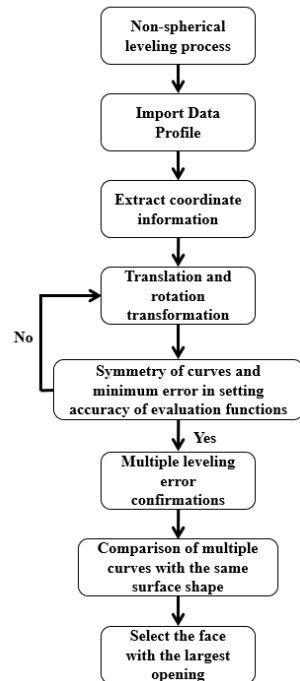


Figure 5. Leveling process flowchart for scanning the curves of the aspheric surface profile.

After data preprocessing and leveling, multiple sets of data are compared to select the optimal group. For an aspheric surface profile, five sets of data are used. By leveling and visualizing the data, multiple measurement datasets are plotted on the same coordinate system for intuitive comparison. From the multiple sets of aspheric surface profile data, the profile data with the “maximum opening” are selected as the best data for aspheric surface scanning. As shown in Figure 7.

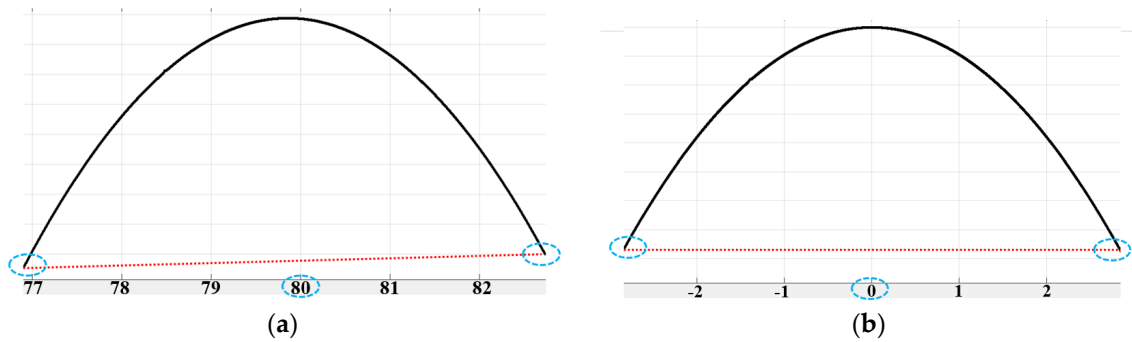


Figure 6. (a,b) show the comparison of curves before and after leveling, respectively. In (a), the blue circle represents the center at the number 80 when not leveled, and the red dotted line indicates that the connection between the two symmetrical points forms a diagonal line. In (b), the blue circle represents the curve being symmetrical about the Y-axis when leveled, and the red dotted line indicates that the connection between the two symmetrical points forms a horizontal line.

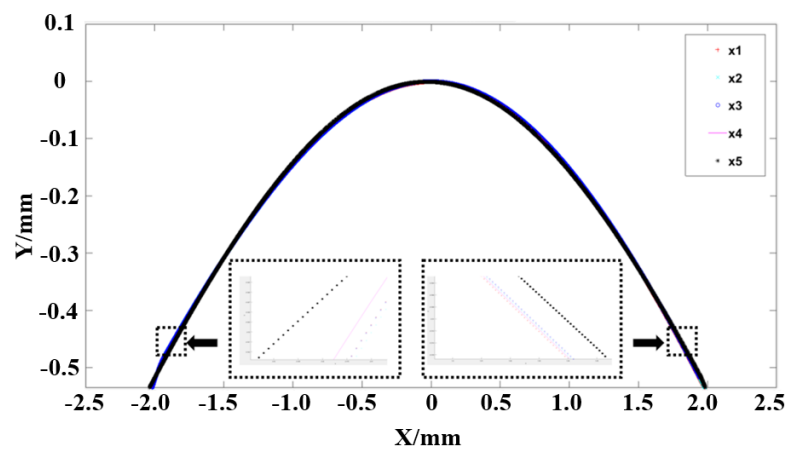


Figure 7. Comparison of curves from five different dataset of the same surface profile.

3.3.2. Fitting Accuracy Evaluation Indicators

Fitting accuracy evaluation indicators are criteria used to determine the quality of fitting results. The results of four evaluation indicators for fitting three types of surface profiles over different ranges are shown in Figure 8.

For the AC111116 and AC90754 aspheric lenses, which have relatively small curvatures, the values of the goodness –of –fit R^2 and adjusted R^2 in the fitting results are almost 1, and are particularly close to 1 in the small interval range of $[-0.1, 0.1]$, indicating good fitting quality. Additionally, in different fitting intervals, the goodness –of –fit metrics SSE and RMSE are close to 0; however, as the fitting interval increases, both the SSE and RMSE also increase, indicating a decline in fitting quality. When the fitting interval approaches the full diameter of the lens, the SSE and RMSE exhibit a clear jump, suggesting that the fitting performance is poor when the fitting interval is the full diameter of the lens. Experimental data indicate that for lenses with small curvatures, selecting half the lens’s full diameter as the fitting interval yields better results.

For the AC91558 aspheric lens, which has a relatively large curvature, the values of the goodness –of –fit R^2 and adjusted R^2 are 1 when a larger fitting interval range is chosen, and close to 1 when a smaller fitting interval is selected, indicating good fitting quality. Moreover, in the different fitting intervals, the goodness –of –fit metrics SSE and RMSE are close to 0, but they increase as the fitting interval expands, leading to a decline in the surface fitting quality, indicating poor fitting performance for the curvature radius. Therefore, to ensure the reliability of the curvature radius fitting results, it is essential to select a suitably small fitting interval range.

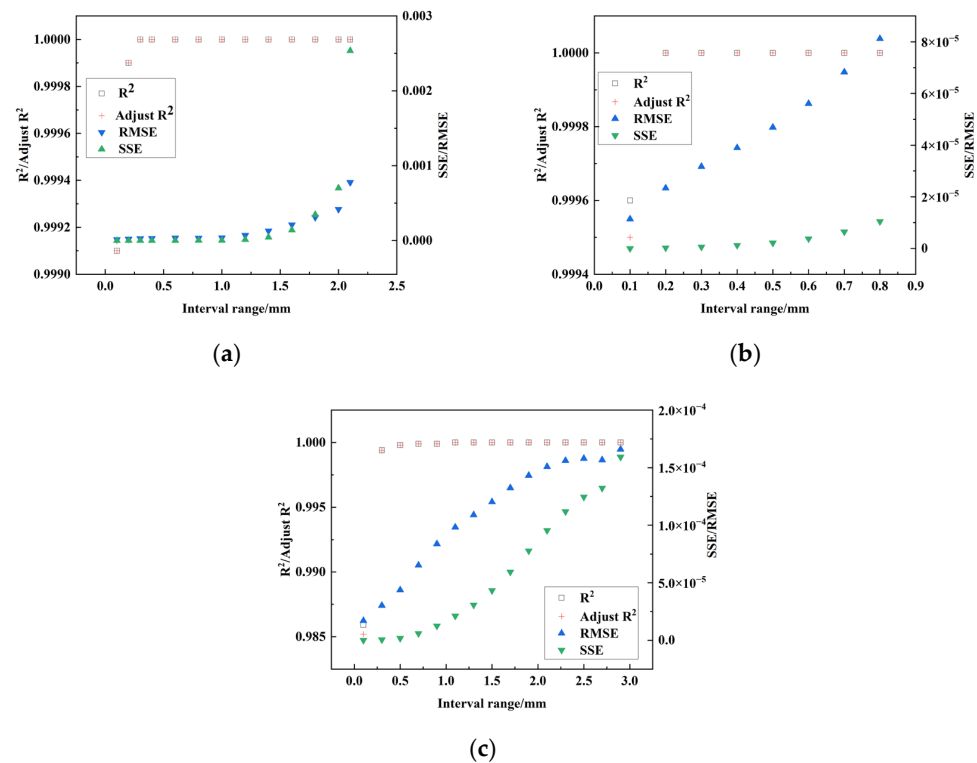


Figure 8. (a–c) represent the results of four evaluation indicators for the AC111116 lens, AC90754 lens, and AC91558 lens, respectively, under different fitting diameters.

3.3.3. Surface Profile Fitting

Due to the differences in sample surface profiles, some fitting processes cannot be completed in one step. This requires adjustments such as changing the fitting interval and re-selecting the iterative algorithm. Additionally, some data may need to be re-leveled and preprocessed to achieve high-precision curvature fitting. After completing the preprocessing of measurement results, valid data should be selected, and excess portions of the surface profile curve should be excluded, such as the stepped areas outside the edges of the surface profile curve. Appropriate iterative algorithms and result criteria should be selected for fitting. Different aspheric surface profiles require different fitting intervals, as the choice of fitting interval will also affect fitting accuracy. The flowchart for aspheric fitting is shown in Figure 9. The fitting results are shown in Figure 10.

The AC111116 lens has symmetrical front and back surfaces, with the curvature radii being equal in magnitude, but opposite in sign. Therefore, in this experiment, we fitted its front surface and obtained the curvature for different fitting intervals. During the aspheric fitting process, the overall fitted curvature radius values maintained measurement repeatability within an acceptable error range. To improve the accuracy of the measurement results, it is crucial to choose the optimal fitting interval that minimizes errors. For surfaces with relatively small curvature, we observed from the fitting data that under the small interval of $[-0.1, 0.1]$, the maximum fitting error reached 0.057977 mm, resulting in significant error impact. When using a larger fitting interval, since the aspheric diameter is 4.2 mm, if the fitting interval is set to $[-2.1 \text{ mm}, 2.1 \text{ mm}]$, which corresponds to the aspheric fitting diameter of 4.2 mm, the error is not at its maximum. However, the evaluation metrics SSE and RMSE are relatively large, indicating decreased fitting quality. Thus, for aspheric lenses with smaller curvature, using a fitting interval that is slightly less than 50% of the aspheric diameter yields a fitting error of 0.013912 mm. At this point, the fitting quality is also considerable, reducing the fitting error by about three times compared to the smaller

diameter case, and the error caused by substituting into the Zemax numerical model will also be minimized.

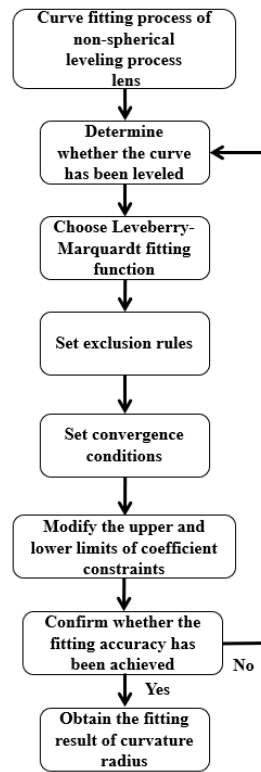


Figure 9. Flowchart for aspheric surface profile curve fitting.

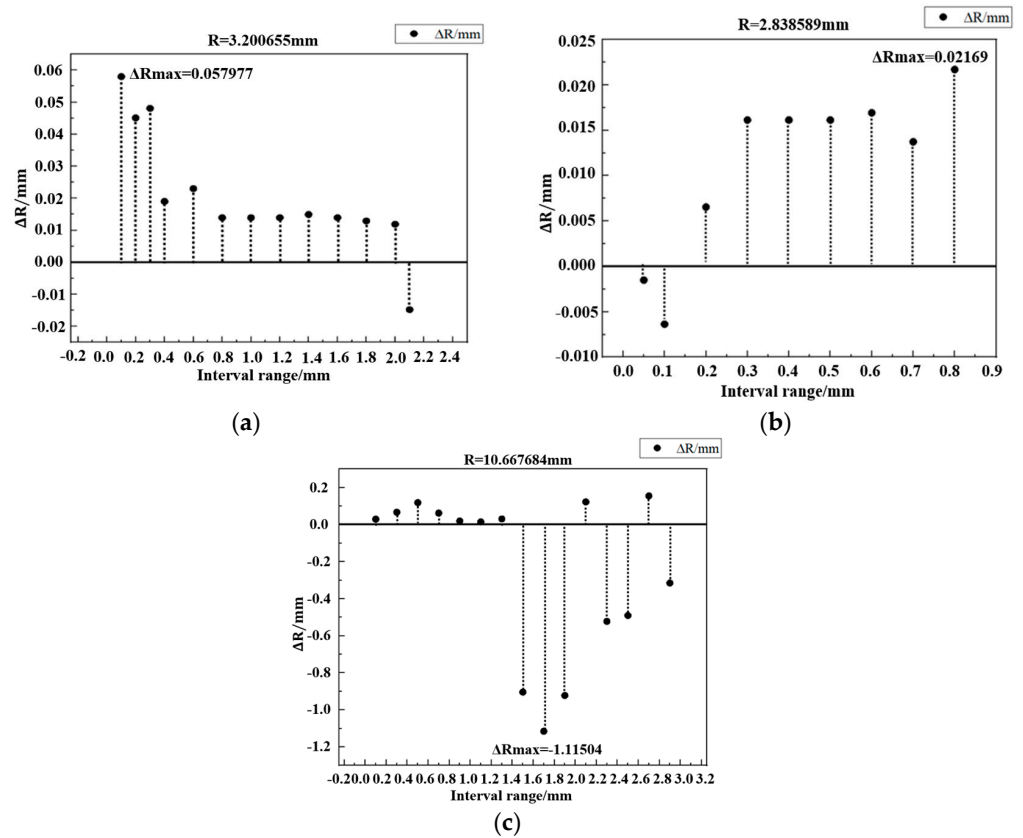


Figure 10. (a–c) represent the curvature radius of the AC111116 lens, AC90754 lens, and AC91558 lens at different fitting interval ranges, respectively.

For the AC90754 lens, the ΔR is small during small interval fittings. However, as can be seen from Figure 9, the fitting quality for R^2 and adjusted R^2 is poor, so this is not considered a reference fitting interval. In the larger fitting range of $[-0.8, 0.8]$, the maximum fitting error reaches 0.02169 mm. In contrast, when fitting using a 50% full diameter interval, the resulting error is small, and the fitting quality is good.

The AC91558 lens has a greater curvature profile. When choosing a large fitting interval, the fitting errors for the curvature radius are relatively large, with the maximum fitting error reaching -1.11504 mm. However, using a smaller fitting interval results in smaller errors, with the minimum error being 0.014653 mm in the fitting interval of $[-1.1, 1.1]$, and the fitting quality is also good. Therefore, for aspheric lenses with a smooth central region and larger curvature, selecting a small diameter fitting interval improves fitting accuracy, yielding more accurate curvature radius.

3.4. Refractive Index Recovery Verification

For the process of reconstructing the refractive index model, the focal length of the aspheric lens and the curvature radius of its aspheric surface profile have been obtained through the previous analysis. The central thickness parameter of the unknown lens is acquired through CT scanning, and the measurement accuracy of the thickness achieved by CT scanning can reach the millimeter level, rendering the error induced in the recovered refractive index negligible.

The accuracy of refractive index recovery is determined by the measurement accuracy of the focal length and the fitting accuracy of the curvature radius. The fitting results are shown in Figure 11. Therefore, the precision of refractive index recovery needs to utilize the focal length measurement data and the surface fitting results to reconstruct the model of the aspheric lens through Zemax. The fitting results are shown in Figure 12. Finally, the recovered refractive index is compared with the actual refractive index.

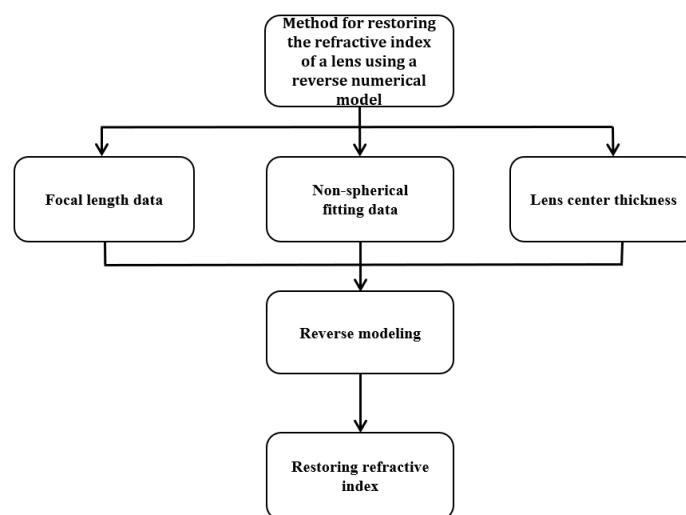


Figure 11. Flowchart for recovering the refractive index of the lens.

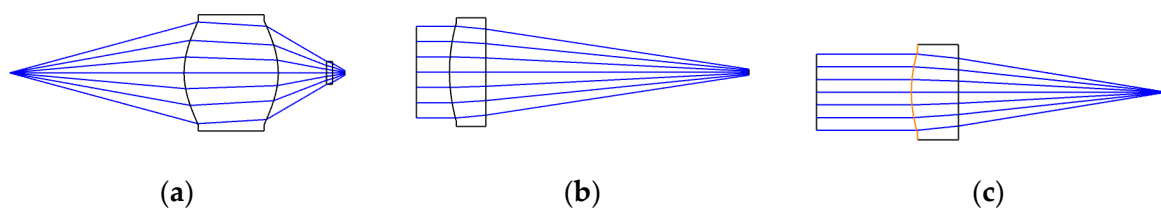


Figure 12. Figures (a–c) represent the reconstructed models of the aspheric lenses AC111116, AC90754, and AC91558, respectively.

For plano-convex (or plano-concave) lenses, since the curvature of one side is infinite, Equation (6) can be simplified to Equation (8):

$$\frac{1}{f} = (n - 1)/R \quad (8)$$

The focal length and refractive index are the core influencing factors in the process of numerically simulating the recovery of the refractive index. To investigate the errors in the recovered refractive index caused by measurement errors in the focal length and fitting errors in the curvature radius, we can derive the partial derivatives of both the curvature radius and focal length using the thick lens formula in Equation (8). The partial differential equations are given in Equations (9) and (10):

$$\frac{\partial n}{\partial R} = \frac{1}{f} \quad (9)$$

$$\frac{\partial n}{\partial f} = \frac{n - 1}{f} \quad (10)$$

The refractive index range of commonly used optical plastics for lens manufacturing is between 1.492 and 1.681, while the refractive index of glass materials for lenses is also less than 2. From this, we can derive that $\frac{\partial n}{\partial R} = \frac{1}{f} > \frac{\partial n}{\partial f} = \frac{n-1}{f}$, indicating that the accuracy of the curvature radius fitting has the greatest impact on the refractive index. For biconvex or biconcave samples, both surfaces have curvature, so the effect of the curvature radius on the refractive index is even more significant. The measurement accuracy of the focal length is 1.06%, thus the impact of the focal length on the refractive index recovery error can be considered negligible. The results are presented in Table 1.

Table 1. Fitting errors of radius of curvature and errors in recovered refractive index.

Sample	True Radius of Curvature (mm)	Fitted Radius of Curvature (mm)	Fitting Error of Radius of Curvature (mm)	True Refractive Index	Recovered Refractive Index	Recovery Accuracy of Refractive Index
AC111116	3.2007 −3.2007	3.1868 −3.1868	0.0139 −0.0139	1.8058	1.8024	0.188%
AC90754	2.8386 PLANO	2.8225 -	0.0161 -	1.58642	1.58643	$6.303 \times 10^{-4}\%$
AC91558	10.6677 PLANO	10.6530 -	0.0147 -	1.5864	1.5856	0.0504%

From the data in the tables, it can be seen that when an appropriate fitting interval is selected, the fitting error of the radius of curvature is small, and the recovery error of the refractive index is also small. The recovery error for the AC111116 lens is 0.0034, the refractive index recovery error for the AC90754 lens is 1×10^{-5} , and the refractive index recovery error for the AC91558 lens is 0.0008. However, in the actual fitting process, for different surface shapes, selecting an appropriate fitting interval allows for obtaining a radius of curvature with a smaller fitting error. Furthermore, when measuring aspheric surface data, the accuracy improves with higher leveling precision, which in turn enhances the recovery precision of the refractive index.

4. Conclusions

In the forward design process of aspheric lenses, specific focal lengths can be obtained by designing the radius of curvature and the refractive index of the materials. This paper presents a method for reverse numerical simulation of material refractive index recovery, given the focal length and the radius of curvature of the aspheric lens surface, which can guide existing parameter design issues during the actual manufacturing process. The recovery precision varies for different surface shapes, with the fitting precision of the radius of curvature reaching a maximum of 0.138%, and the accuracy of refractive index recovery reaching a maximum of $6.303 \times 10^{-4}\%$. Additionally, by measuring the focal lengths at three wavelengths, the Abbe number of the lens can be derived using the dispersion formula, which can further lead to identifying the specific material of unknown samples.

Author Contributions: Conceptualization, T.Z. (Tao Zhong) and G.G.; methodology, T.Z. (Tao Zhong); software, Y.C.; validation, T.Z. (Tao Zhong), G.G. and Y.Y.; formal analysis, J.Y. and G.G.; investigation, T.Z. (Tao Zhong) and T.J.; resources, M.L. and Y.W.; data curation, Y.Z. and Y.S.; writing—original draft preparation, T.Z. (Tao Zhong) and G.G.; writing—review and editing, T.Z. (Tao Zhong) and G.G.; visualization, T.Z. (Tianhao Zhong) and G.G.; supervision, Y.S. and C.K.; project administration, G.G.; funding acquisition, G.G. All authors have read and agreed to the published version of the manuscript.

Funding: This research was supported by the fund of the National Key Research and Development Program of China (2021YFB3601403), the Scientific and Technology Research Program of Chongqing Municipal Education Commission (KJQN202300527), and the National Natural Science Foundation of China (62205041).

Data Availability Statement: The study did not report any data.

Conflicts of Interest: The authors declare no conflict of interest.

References

1. Meyzonnette, J.-L.; Mangin, J.; Cathelinaud, M. Refractive Index of Optical Materials. In *Springer Handbook of Glass*; Springer Handbooks book series (SHB); Springer: Cham, Switzerland, 2019; pp. 997–1045. [[CrossRef](#)]
2. Smith, G. Liquid immersion method for the measurement of the refractive index of a simple lens. *Appl. Opt.* **1982**, *21*, 755–757. [[CrossRef](#)] [[PubMed](#)]
3. Kasana, R.S.; Rosenbruch, K.J. Determination of the refractive index of a lens using the murty shearing interferometer. *Appl. Opt.* **1983**, *22*, 3526–3531. [[CrossRef](#)] [[PubMed](#)]
4. Soni, K.; Kasana, R.S. The use of defocused position of a ronchi grating for evaluating the refractive index of lens. *Opt. Laser Technol.* **2007**, *39*, 1334–1338. [[CrossRef](#)]
5. Soni, K.; Kasana, R.S. The role of an acousto-optic grating in determining the refractive index of a lens. *Meas. Sci. Technol.* **2007**, *18*, 1667–1671. [[CrossRef](#)]
6. Kasana, R.S.; Goswami, A.; Soni, K. Non-destructive multiple beam interferometric technique for measuring the refractive indices of lenses. *Opt. Commun.* **2004**, *236*, 289–294. [[CrossRef](#)]
7. Glatt, I.; Livnat, A. Determination of the refractive index of a lens using moire deflectometry. *Appl. Opt.* **1984**, *23*, 2241–2243. [[CrossRef](#)] [[PubMed](#)]
8. Kasana, R.S.; Boseck, S.; Rosenbruch, K.J. Use of a grating in a coherent optical-processing configuration for evaluating the refractive index of a lens. *Appl. Opt.* **1984**, *23*, 757–761. [[CrossRef](#)] [[PubMed](#)]
9. Nussbaumer, R.J.; Halter, M.; Tervoort, T.; Caseri, W.R.; Smith, P. A simple method for the determination of refractive indices of (rough) transparent solids. *J. Mater. Sci.* **2005**, *40*, 575–582. [[CrossRef](#)]
10. Fu, J.; Zheng, S.; Xie, F. Research on the Application of Rotational Quadratic Surface Imaging in Physics Teaching. *J. Shangqiu Norm. Univ.* **2003**, *19*, 6.
11. Xu, J.; Gu, J.; Zhang, L. Determination of the Curvature Radius and Refractive Index of a Biconcave Thick Lens. *J. Univ. Phys. Exp.* **2011**, *24*, 3.
12. Chen, L.; Guo, X.; Hao, J. Lens refractive index measurement based on fiber point-diffraction longitudinal interferometry. *Opt. Express* **2013**, *21*, 22389–22399. [[CrossRef](#)] [[PubMed](#)]

13. Ford, H.D.; Francis, D.; Hallam, J.M.; Tatam, R.P. Influence of aberrations on confocal-based remote refractive index measurements. *Appl. Opt.* **2019**, *58*, 6474. [[CrossRef](#)] [[PubMed](#)]
14. Chhaniwal, V.K.; Anand, A.; Narayanamurthy, C.S. Determination of refractive indices of biconvex lenses by use of a michelson interferometer. *Appl. Opt.* **2006**, *45*, 3985–3990. [[CrossRef](#)] [[PubMed](#)]
15. Anand, A.; Chhaniwal, V.K. Measurement of parameters of simple lenses using digital holographic interferometry and a synthetic reference wave. *Appl. Opt.* **2007**, *46*, 2022–2026. [[CrossRef](#)] [[PubMed](#)]
16. Zhao, W.; Wang, Y.; Qiu, L.; Guo, H. Laser differential confocal lens refractive index measurement. *Appl. Opt.* **2011**, *50*, 4769–4778. [[CrossRef](#)] [[PubMed](#)]

Disclaimer/Publisher’s Note: The statements, opinions and data contained in all publications are solely those of the individual author(s) and contributor(s) and not of MDPI and/or the editor(s). MDPI and/or the editor(s) disclaim responsibility for any injury to people or property resulting from any ideas, methods, instructions or products referred to in the content.